

Overcalcified forms of the coccolithophore *Emiliana huxleyi* in high CO₂ waters are not pre-adapted to ocean acidification.

Peter von Dassow^{1,2,3*}, Francisco Díaz-Rosas^{1,2}, El Mahdi Bendif⁴, Juan-Diego Gaitán-Espitia⁵, Daniella Mella-Flores¹, Sebastian Rokitta⁶, Uwe John⁶, and Rodrigo Torres^{7,8}

¹ Facultad de Ciencias Biológicas, Pontificia Universidad Católica de Chile, Santiago, Chile.

² Instituto Milenio de Oceanografía de Chile.

³ UMI 3614, Evolutionary Biology and Ecology of Algae, CNRS-UPMC Sorbonne Universités, PUCCh, UACH.

⁴ Department of Plant Sciences, University of Oxford, OX1 3RB Oxford, UK.

⁵ CSIRO Oceans and Atmosphere, GPO Box 1538, Hobart 7001, TAS, Australia.

⁶ Marine Biogeosciences | PhytoChange Alfred Wegener Institute – Helmholtz Centre for Polar and Marine Research, Bremerhaven, Germany.

⁷ Centro de Investigación en Ecosistemas de la Patagonia (CIEP), Coyhaique, Chile.

⁸ Centro de Investigación: Dinámica de Ecosistemas marinos de Altas Latitudes (IDEAL), Punta Arenas, Chile.

Correspondence to: Peter von Dassow (pvondassow@bio.puc.cl)

SUPPLEMENTARY MATERIALS

Supplementary Section S1

Variation in relative abundance of E. huxleyi morphotypes with depth.

We note that the dominant morphotype of *Emiliana huxleyi* was usually the same at the surface and deeper in the water column (Fig. S1-S2). One exception was a station near Punta Lengua de Vaca (Tongoy Station 18) where lightly calcified morphotypes dominated below the thermocline and R/overcalcified morphotypes dominated above (Fig. S1f). Another exception was the station 2 in the JF survey, where the lightly calcified morphotypes were dominant within and below the picnocline but the A morphotype was dominant, although at the lower total abundance (Fig. S1h). Table S3 (Supplementary section S3) gives abundances with depth at the stations shown in Fig. S1-S2.

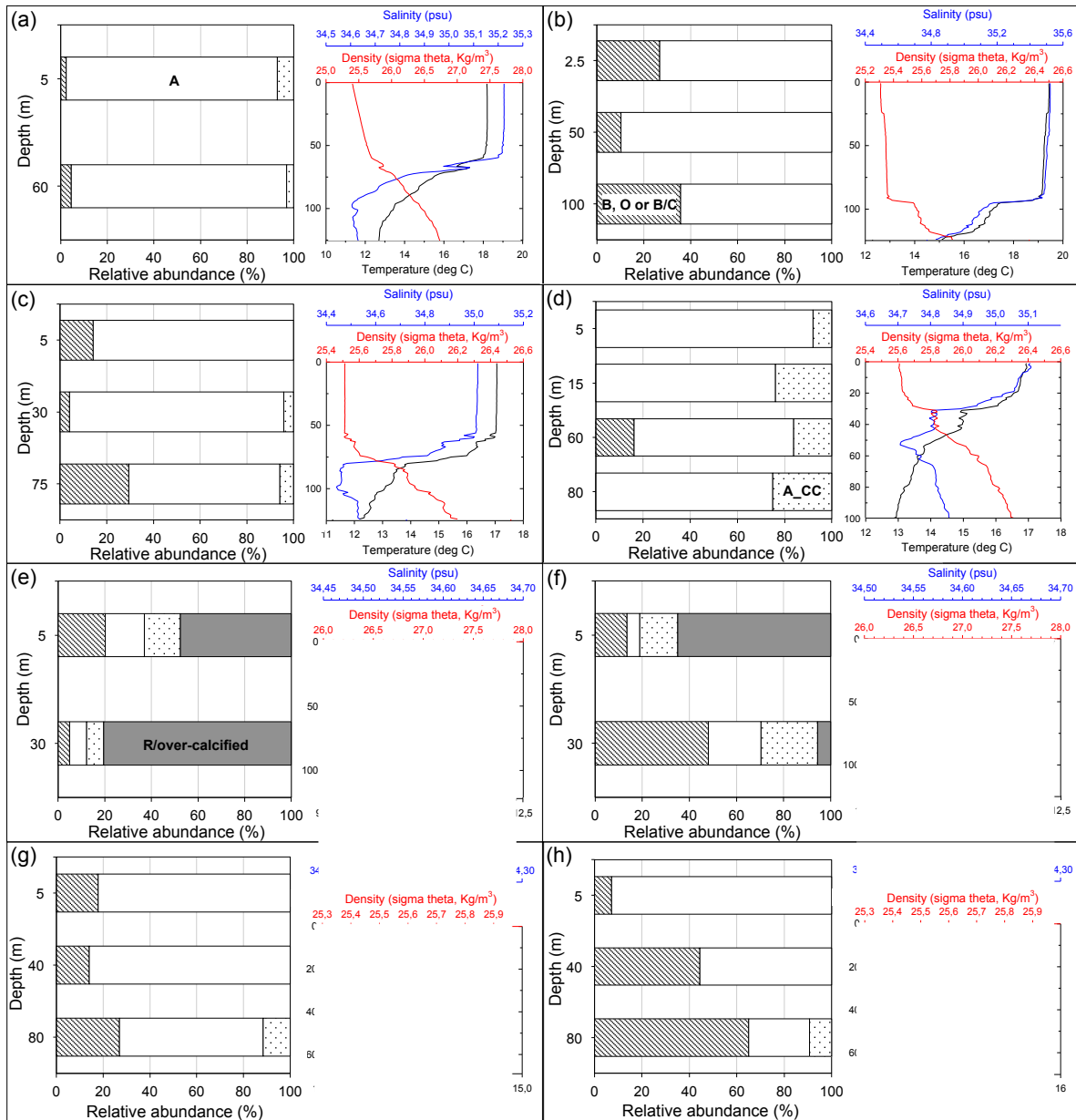


Figure S1. Relative abundances of *Emiliana huxleyi* morphotypes in the upper water column by study site. In a-d), e-f) and g-h) the relative abundances yielded by *E. huxleyi* morphotypes in NBP cruise (st. H04, H13, H19, BB2f), Tongoy Bay (st. 01 and 18) and Juan Fernandez surveys (st. 01, 02) are shown, respectively. Temperature (black), salinity (blue) and density (red) profiles for each station are shown at the right. Morphotypes are indicated on the bars.

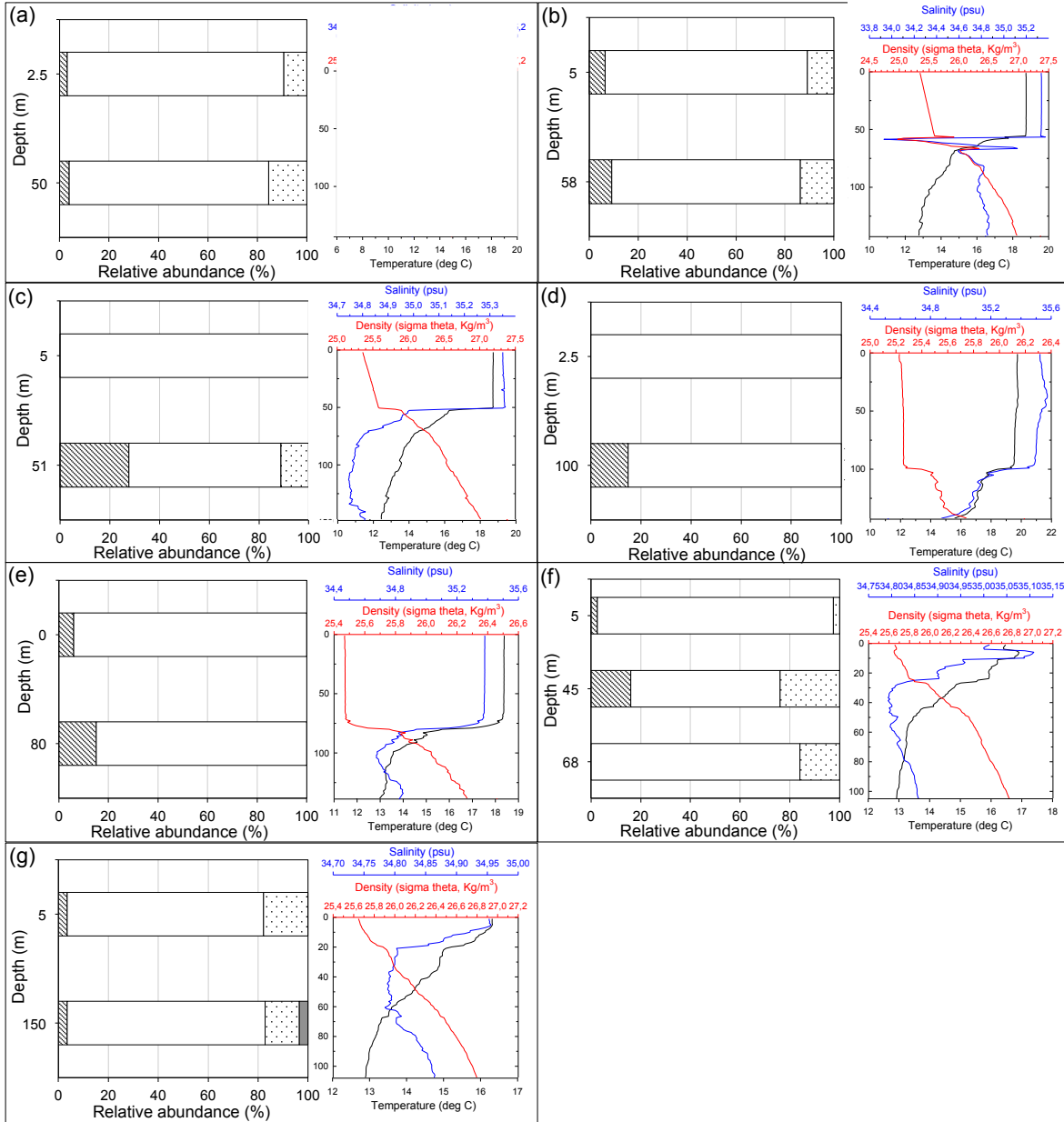


Figure S2. Relative abundances of *Emiliana huxleyi* morphotypes in the upper water column. In a-g) the relative abundances yielded by *E. huxleyi* morphotypes in NBP cruise (st. H01, BB1a, BB1b, H10, H17, BB2b, BB2c) are shown in panels a-g. Temperature (black), salinity (blue) and density (red) profiles for each station are shown at the right. Morphotypes are as in Fig. S1. A conductivity sensor error in BB1a caused a spike that was not filtered out successfully.

Supplementary Section S2

*Redundancy analysis (RDA) methodology used and RDA results for *Emiliana huxleyi* morphotype distributions constrained by environmental variables.*

To determine the abiotic variables driving the *Emiliana huxleyi* populations a redundancy analysis (RDA) was performed (rda function in vegan package Oksanen et al., 2007, performed in RStudio version 1.0.143 for mac OS). RDA is a direct constrained method that combine multivariate multiple linear regression with principal component analysis (Borcard et al., 2011). To RDA analyses we followed the methodology provide by Borcard et al. (2011). The variation in *E. huxleyi* morphotypes (matrix composed by relative abundances) were regressed on environmental conditions (temperature, salinity and $p\text{CO}_2$), while controlling for sampling location (vector of offshore distances in km). To test for significance of RDA model and axis the pseudo-F statistic was calculated by set a minimal number of 1,000 sample permutations (Borcard et al., 2011). As linear dependencies between environmental variables can inflated the regression coefficient (Borcard et al., 2011), variance inflation factors were checked after each RDA analysis (vif.cca function in vegan package). RDA results are plotted in Fig. S3.

References.

Borcard, D., Gillet, F. and Legendre, P. 2011. Numerical ecology with R. Springer Science+Business Media. pp. 306.

Oksanen, J., Blanchet, F., Kindt, R., Legendre, P., Minchin, P., O'Hara, R., Simpson, G., Solymos, P., Stevens, M. and Wagner, H. 2007. Vegan: Community Ecology Package. R package version 2.3-1. Available at: <https://cran.r-project.org/web/packages/vegan/index.html> (last accessed 16 July 2017).

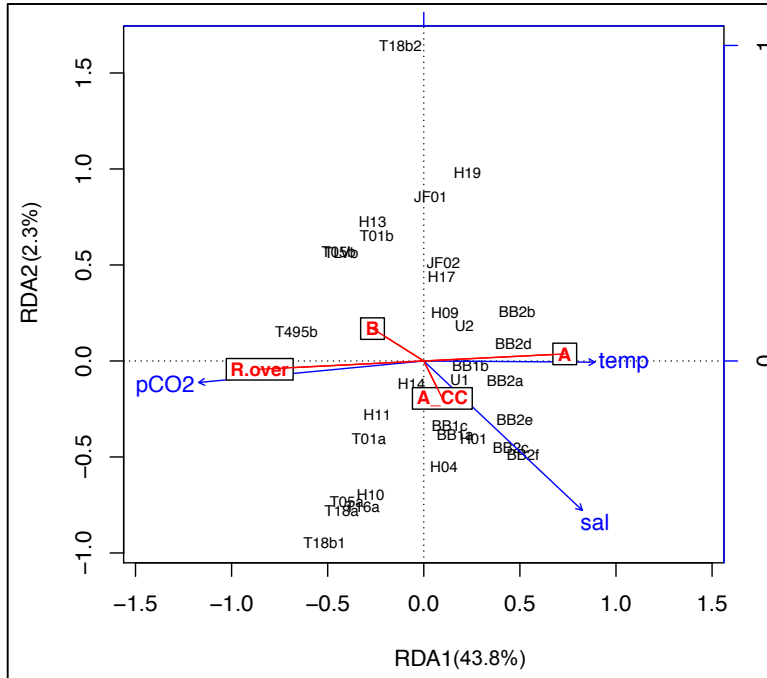


Figure S3. Redundancy analysis results for *Emiliana huxleyi* morphotype distributions constrained by environmental variables. The relative abundances of *E. huxleyi* morphotypes (red labels) from surface stations (black labels) were constrained by three environmental variables (blue arrows). Percentage of variance explained by each RDA axis are displayed. Only the first RDA axis appeared to be significant ($p < 0.05$). RDA triplot was performed with site scores and scaling 2.

Supplementary Section S3

Measured alkalinity change versus alkalinity changes predicted from PIC and nutrient consumption.

Precipitation of 1 mole of CaCO_3 should consume 2 moles of alkalinity. Thus there should be a linear relationship between PIC production and alkalinity decrease (Zeebe and Wolf-Gladrow, 2003). In an initial analysis we observed that alkalinity decreases in strain CHC342 at the control (400 μatm) CO_2 treatment were higher than expected ($-421.4 \pm 32.2 \mu\text{mol kg}^{-1}$). Over all strains and all treatments, observed alkalinity decreases were significantly linearly related ($R^2 = 0.594$, $p < 0.0001$ for difference from a slope of 0) to the expected alkalinity decreases calculated as twice the PIC contents (in $\mu\text{mole kg}^{-1}$). However, the slope between observed and expected alkalinity change was significantly greater than 1 (slope 1.54 ± 0.22 , 95% confidence interval 1.09 to 1.99). Visual inspection indicated that all replicates from strain CHC342 at the control CO_2 treatment, and three out of four replicates from strain CHC440 at the control treatment, but no other samples, were above the 95% confidence interval for the regression. We performed the regression again, eliminating all samples of CHC342 and CHC440 (both control and high CO_2 /low pH treatments). In that case, there was also a significant linear relationship between observed and expected alkalinity decreases ($R^2 = 0.73$, $p < 0.0001$), but the slope was not significantly different from 1 (slope 0.89 ± 0.13 , 95% confidence interval 0.62 to 1.17) (curve not shown).

Smaller alkalinity changes are also associated with the uptake of nutrients by phytoplankton (Zeebe and Wolf-Gladrow, 2003): Assuming most phosphate is in the form HPO_4^{2-} at the experimental pH, alkalinity should decrease by one mole for every mole of phosphate consumed. Alkalinity should increase by one mole for every nitrate consumed. Nutrient data is not available (samples were taken but lost in transit). However, when nutrients are not limiting, nitrate and phosphate are consumed (and particulate organic N and particulate organic P is formed) in approximately Redfield ratios with C, while N and P quotas are decreased under nutrient limitation (e.g., Rokitta et al., 2014, 2016). A corrected estimation of expected alkalinity change was calculated as:

$$\text{Expected } \Delta_{\text{alkalinity}} = -2 \times \text{PIC} - \text{POC}/106 + \text{POC}/6.625,$$

where PIC, POC, and alkalinity values are in $\mu\text{mol kg}^{-1}$. This estimation lacks precision. For example, if PIC is underestimated, POC is overestimated, so the correction will be overestimated. However, it aids in determining whether or not the correction could improve the match between expected and observed alkalinity. When all data is considered, the slope is 1.62 ± 0.24 ($R^2 = 0.58$, $p < 0.0001$) (Fig. S4). The slope is significantly greater than one (95% confidence interval 1.13 to 2.11), and the y-intercept is not significantly different from 0 (9.94 ± 22.5 , 95% confidence interval -35.8 to 55.6). When data from strains CHC342 and CHC440 are excluded, there is also a significant relationship, with slope = 0.920 ± 0.140 ($R^2 = 0.717$, $p < 0.0001$) (Fig. S4). The slope is not significantly different from 0 (95% confidence interval 0.62 to 1.22) and the y-intercept is also not significantly different from 0 (-0.96 ± 11.93 , 95% confidence interval -26.1 to 24.2). More importantly, the correction did not decrease the difference between measured and expected alkalinity changes for either strains CHC342 or CHC440 under the control CO_2 /pH condition.

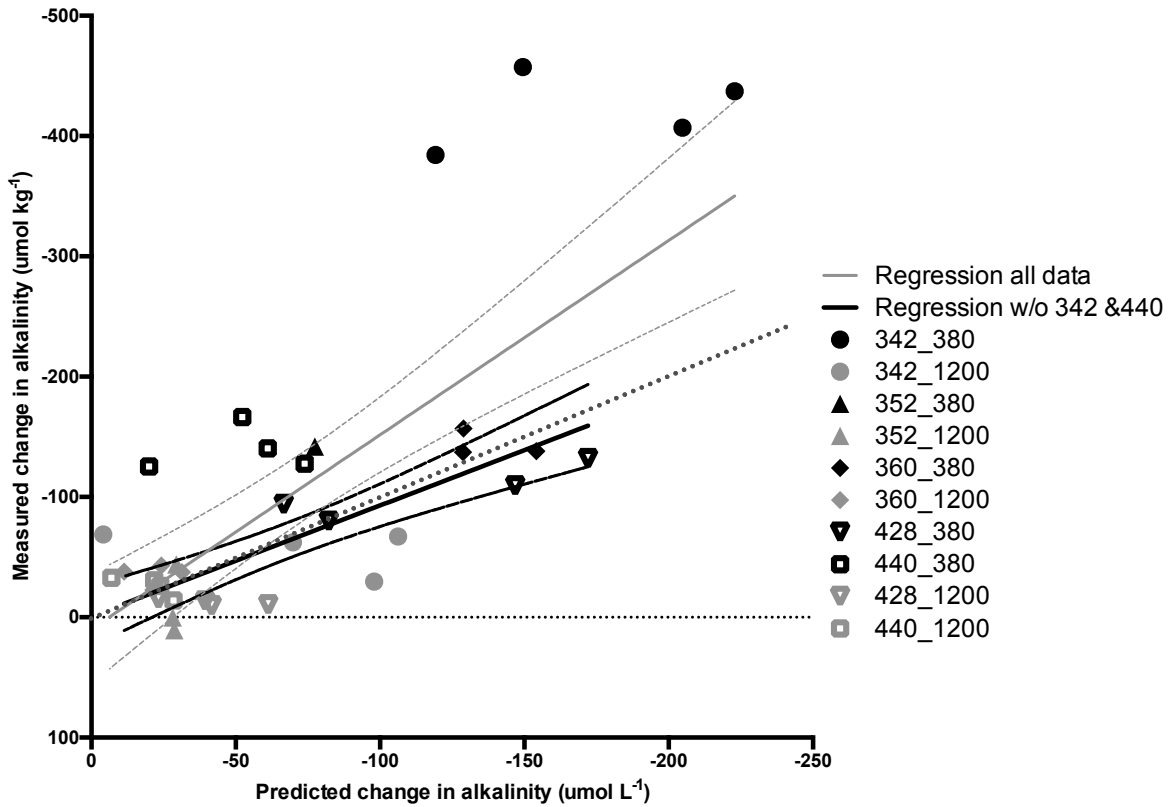


Figure S4. Measured change in alkalinity versus change in alkalinity predicted from measured PIC and POC. The grey continuous line represents the linear regression considering all data, with the grey dashed lines representing the 95% confidence interval of the regression. The black continuous and dashed lines similarly represent the linear regression and 95% confidence interval when data from strains CHC342 and CHC440 is left out. The dotted black line represents the 1:1 relationship between observed and predicted alkalinity change.

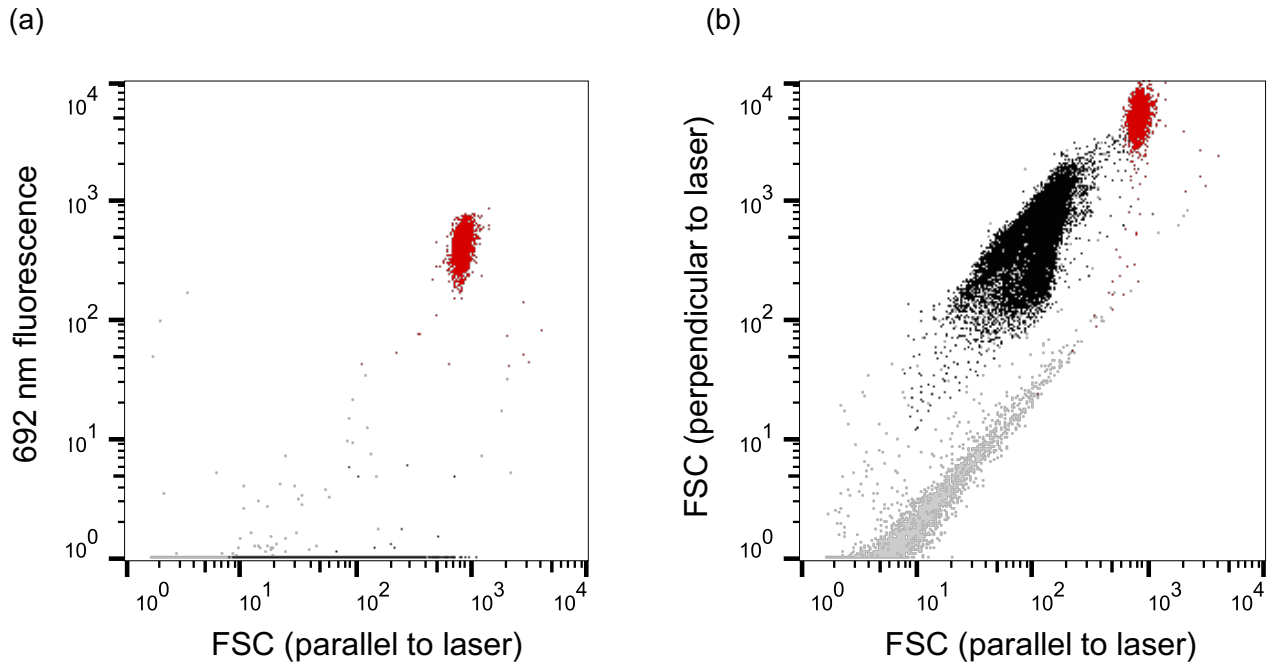


Figure S5: Example flow cytograms (of CHC352 at 400 $\mu\text{atm CO}_2$) showing identification of chlorophyll-containing (red fluorescent cells) in plot of 692 nm (40 nm band pass) fluorescence (y-axis) vs forward scatter with polarization parallel to laser (FSC) (a) and cytogram of scatter depolarization (FSC with polarization perpendicular to laser vs FSC with polarization parallel to laser) (b). Chlorophyll-containing cells are represented by red dots, black dots represent detached coccoliths, and grey dots represent other particles, which are mostly not optically active and fall on a straight line in panel b.